



## Manipulating spectral topology and exceptional points by nonlinearity in non-Hermitian polariton systems

Jan Wingenbach <sup>1</sup>, Stefan Schumacher,<sup>1,2,3</sup> and Xuekai Ma <sup>1</sup>

<sup>1</sup>*Department of Physics and Center for Optoelectronics and Photonics Paderborn, Paderborn University, Warburger Strasse 100, 33098 Paderborn, Germany*

<sup>2</sup>*Institute for Photonic Quantum Systems, Paderborn University, Warburger Straße 100, 33098 Paderborn, Germany*

<sup>3</sup>*Wyant College of Optical Sciences, University of Arizona, Tucson, Arizona 85721, USA*



(Received 9 May 2023; accepted 8 January 2024; published 7 February 2024)

Exceptional points (EPs), with their intriguing spectral topology, have attracted considerable attention in a broad range of physical systems, with potential sensing applications driving much of the present research in this field. Here, we investigate spectral topology and EPs in systems with significant nonlinearity, exemplified by a nonequilibrium exciton-polariton condensate. With the possibility to control loss and gain and nonlinearity by optical means, this system allows for a comprehensive analysis of the interplay of nonlinearities (Kerr type and saturable gain) and non-Hermiticity. Not only do we find that EPs can be intentionally shifted in parameter space by the saturable gain, but we also observe intriguing rotations and intersections of Riemann surfaces and find nonlinearity-enhanced sensing capabilities. With this, our results illustrate the potential of tailoring spectral topology and related phenomena in non-Hermitian systems by nonlinearity.

DOI: [10.1103/PhysRevResearch.6.013148](https://doi.org/10.1103/PhysRevResearch.6.013148)

### I. INTRODUCTION

Exceptional points (EPs) are singularities in parameter space at which two or more eigenvalues and their corresponding eigenvectors coalesce [1–4]. Such singularities occur exclusively in non-Hermitian systems which are subject to gain and loss and exhibit nonorthogonal eigenvectors and complex eigenvalues [5,6]. Compared to conventional singularities in Hermitian systems, known as Diabolic points, EPs show intriguing properties due to the spectral topology of their Riemann surfaces [7,8]. EPs have been widely investigated in a variety of physical systems such as microwave resonators [9–11], atomic systems [12], plasmonic nanostructures [13,14], optical waveguides [15], microresonators [16–18], and nonreciprocal systems [19]. Near an EP, a range of counterintuitive phenomena has been reported in optical systems due to the coalescence of the eigenvectors, including loss- and optomechanically induced transparency [20,21], unidirectional invisibility, and reflectivity exceeding unity [15,22]. Moreover, sensing enhancement can be realized close to an EP of order  $n$  where the frequency splitting scales as the  $n$ th root of the perturbation [23–26]. This makes EPs promising candidates for a new generation of sensors, with the potential to outperform their Hermitian counterparts [27–30].

Recently, there has been growing interest in the interplay of nonlinearity and non-Hermiticity. For instance, the influence of nonlinear effects on the  $\mathcal{PT}$  symmetry in lasing systems

was studied [31–34]. EP-based sensors with saturable gain [35], saturable-gain-induced energy shift [36,37], and the encircling of EPs in bistable domains [38] were investigated. To systematically study the interplay of nonlinear and non-Hermitian physics, systems with variable nonlinearity and controllable gain and loss are required. An example of such systems is exciton polaritons, in which rich nonlinear physics have been reported, such as nonlinear emission [39], stimulation of photoluminescence [40], angle-resonant amplification [41,42], and strong stimulated scattering under resonant excitation [43].

Exciton polaritons are hybrid light-matter quasiparticles that form due to strong light-matter coupling, pairing finite lifetimes on a picosecond scale, and thus non-Hermiticity, with strong nonlinearity from polariton-polariton interactions. For nonresonant optical excitation, spontaneous macroscopic coherence can form, known as polariton condensation [44–46]. In that case, the significant interaction of the condensate and the exciton reservoir induces a repulsive potential energy landscape, enabling optical trapping [47–51] as well as the optical control of the polariton condensate [52–56]. Moreover, the nonlinearity of polariton condensates permits multistabilities [57–60] and hence offers new design avenues for all-optical transistors [61] and allows for the creation and control of vortices [56,62,63]. The nonlinearity inside the polariton condensate can be tuned with static electric fields [64–66]. With their nonequilibrium nature and the possibility of both structural and optical control, polariton systems offer a natural playground for the study of non-Hermitian physics. For instance, non-Hermitian topological corner modes [67], topological interface states [68],  $\mathcal{PT}$  symmetry [69], and EPs [70–74] have been investigated. Moreover, the first measurement of the quantum metric in a non-Hermitian system was

Published by the American Physical Society under the terms of the [Creative Commons Attribution 4.0 International](https://creativecommons.org/licenses/by/4.0/) license. Further distribution of this work must maintain attribution to the author(s) and the published article's title, journal citation, and DOI.

conducted on exciton-polariton eigenstates [75]. However, the interplay of nonlinearity and non-Hermiticity has not been fully explored or exploited.

In the present work, we investigate the manipulation of EPs and surrounding Riemann surfaces through the nonlinearities in the system. We find that the saturable gain shifts the EP in parameter space, leading to a variation in the mode coupling requirement for the observation of the EP. The repulsive polariton-polariton nonlinearity (akin to a Kerr-type nonlinearity) can induce not only an energy blueshift but also a simultaneous rotation of the Riemann surface and movement of the EP. We show that this also applies to higher-order EPs where the Riemann surfaces can show complex intersection patterns. With potential applications in mind, we further demonstrate that sensing sensitivity near the EP can be significantly enhanced by nonlinearity.

## II. THEORETICAL MODEL

To study the dynamics of polariton condensates under non-resonant excitation, we use the dissipative Gross-Pitaevskii (GP) model [63,76]. Within this framework, the dynamics of the coherent polariton field  $\psi = \psi(\mathbf{r}, t)$  and the density of the exciton reservoir  $n = n(\mathbf{r}, t)$  are

$$i\hbar \frac{\partial}{\partial t} \psi = \left( H_0(\mathbf{r}) + g_c |\psi|^2 + g_r n + \frac{i\hbar}{2} [Rn - \gamma_c] \right) \psi, \quad (1)$$

$$\frac{\partial n}{\partial t} = P(\mathbf{r}) - (\gamma_r + R|\psi|^2)n.$$

The linear operator  $H_0(\mathbf{r}) = -\frac{\hbar^2}{2m_{\text{eff}}}\nabla^2 + V(\mathbf{r})$  describes the kinetic energy and the external potential  $V(\mathbf{r})$  which confines the condensate spatially.  $m_{\text{eff}} = 10^{-4}m_e$  is the effective polariton mass, with  $m_e$  being the free electron mass.  $g_c$  is the strength of the polariton-polariton interaction (akin to a Kerr-type nonlinearity), while  $g_r$  is the strength of the polariton-reservoir interaction.  $\gamma_c = 0.3 \text{ ps}^{-1}$  is the loss constant of the condensate in the quasimode approximation [77], counteracted by the stimulated in-scattering with  $R = 0.01 \text{ ps}^{-1} \mu\text{m}^2$ .  $\gamma_r = 0.45 \text{ ps}^{-1}$  is the loss constant of the reservoir, supplemented by the incoherent pump  $P(\mathbf{r})$ . For stationary excitation and solution we obtain  $n(\mathbf{r}) = \frac{P(\mathbf{r})}{\gamma_r + R|\psi(\mathbf{r})|^2}$ ; the term  $R|\psi(\mathbf{r})|^2$  holds the saturable gain.

A system containing an EP of two coalescing eigenvectors is approximated in its vicinity by a two-level effective Hamiltonian,

$$H_{\text{EP2}} = \begin{pmatrix} E_\alpha + i\Gamma_\alpha & \mu/2 \\ \mu/2 & E_\beta + i\Gamma_\beta \end{pmatrix}. \quad (2)$$

Here,  $E_\alpha$  and  $E_\beta$  are the energies of modes  $\alpha$  and  $\beta$ . The gain and loss are included in  $\Gamma_\alpha$  and  $\Gamma_\beta$ , and  $\mu$  characterizes the coupling strength of the two modes. The eigenvalues of the Hamiltonian (2) read  $E_\pm = [E_\alpha + E_\beta + i(\Gamma_\alpha + \Gamma_\beta)]/2 \pm \sqrt{|\mu|^2 + [E_\alpha - E_\beta + i(\Gamma_\alpha - \Gamma_\beta)]^2}/2$ . The second term describes the energy splitting on one side of the EP, which shows the characteristic square-root dependence. Plotting the eigenvalues depending on the energy difference  $\Delta E_L = E_\alpha - E_\beta$  and the loss and gain difference  $\Delta\Gamma = \Gamma_\alpha - \Gamma_\beta$  visualizes the Riemann surface of the system, as shown in Fig. 1(a) for the real part. The EP is localized at  $\Delta E_L = 0$  and  $\mu = \Delta\Gamma$ .

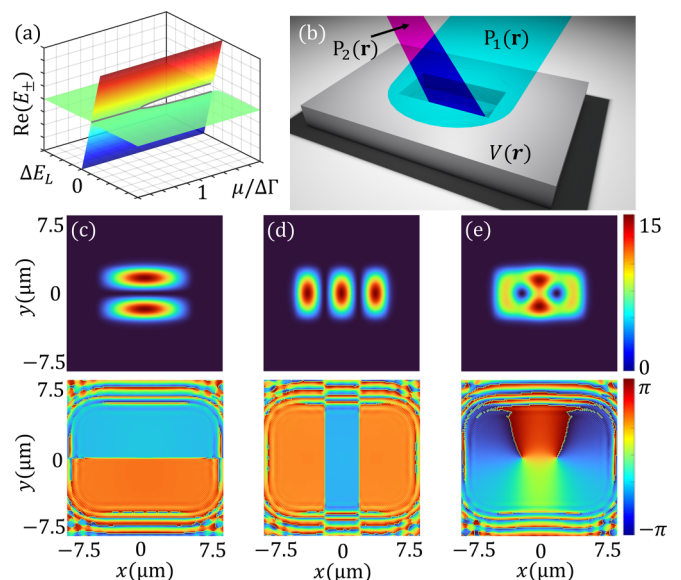


FIG. 1. System and excitation setup. (a) Sketch of the Riemann surface (real part only) of a two-level non-Hermitian system containing an EP for varying level separation  $\Delta E_L = E_\alpha - E_\beta$  and varying relative level coupling  $\mu/\Delta\Gamma$ . (b) Scheme for realization with polariton condensates, including the rectangular external potential  $V(\mathbf{r})$  and excitation with two nonresonant pump beams,  $P_1(\mathbf{r})$  and  $P_2(\mathbf{r})$ . Polariton density (top row; in  $\mu\text{m}^{-2}$ ) and phase (bottom row) of the (c) third and (d) fourth modes of the potential  $V(\mathbf{r})$  that are chosen here as an example for the realization of an EP. (e) Vortex-antivortex mode at the EP. Further details are given in the text.

To study the dynamics of two coupled modes  $\psi_{\alpha,\beta}$  of a polariton condensate in the vicinity of an EP, we extend the effective non-Hermitian Hamiltonian (2) by including the nonlinearity of the GP model. Consequently, the two-level non-Hermitian Hamiltonian and the effective nonlinear Schrödinger equation (NSE) read

$$i\hbar \frac{\partial}{\partial t} \begin{pmatrix} \psi_\alpha \\ \psi_\beta \end{pmatrix} = \begin{pmatrix} H(\psi_\alpha) & \mu/2 \\ \mu/2 & H(\psi_\beta) \end{pmatrix} \begin{pmatrix} \psi_\alpha \\ \psi_\beta \end{pmatrix}, \quad (3)$$

where  $H(\psi) = H_0(\mathbf{r}) + g_c |\psi|^2 + g_r n + \frac{i\hbar}{2} [Rn - \gamma_c]$ . It should be noted that this model can also be applied to other nonlinear systems by substituting the Hamiltonian. In the further course of this work, the eigenenergies of the system are denoted by  $E_{\alpha,\beta}$ , and their difference is denoted by  $\Delta E_L$ . The blueshift-induced correction to this difference is defined as  $\Delta E_{\text{NL}}$ , such that the energy difference in the nonlinear regime is  $\Delta\mathcal{E} = \Delta E_L + \Delta E_{\text{NL}} = \mathcal{E}_\alpha - \mathcal{E}_\beta$ . In this work, we investigate the third,  $\alpha = 3$ , and fourth,  $\beta = 4$ , modes [as shown in Figs. 1(c) and 1(d)] of a rectangular external potential with a width of  $5 \mu\text{m}$ , length of  $8.9 \mu\text{m}$ , and depth of  $2 \text{ meV}$ , as sketched in Fig. 1(b). These two modes are chosen because their energies are close to each other and their degeneracies can be realized in experiments. Provided these conditions are fulfilled, the model can be applied to arbitrary modes [70]. We use a nonresonant pump  $P(\mathbf{r})$  which consists of a broad flat top pump  $P_1(\mathbf{r})$  [light blue cone in Fig. 1(b)] with a diameter of  $12 \mu\text{m}$  and intensity of  $I_1 = 16 \text{ ps}^{-1} \mu\text{m}^{-2}$ . An additional elliptical pump  $P_2(\mathbf{r})$  [light pink cone in Fig. 1(b)] with a height of

$2\ \mu\text{m}$  and width of  $5\ \mu\text{m}$  is used to tune the mode energy difference  $\Delta\mathcal{E}$ . Mathematical expressions for the pump profiles are given in Appendix A 2. The total energies  $\mathcal{E}_{\alpha,\beta}$  of the two modes are obtained by solving the GP equation, Eq. (1), on a discrete spatial grid using the Dormand-Prince method for the time integration and time-domain Fourier transformation for the respective steady states [Figs. 1(c) and 1(d)]. Their scalar gain and loss rates can be approximated by  $\Gamma_{\alpha,\beta} \approx N^{-1} \frac{\hbar}{2} \int [Rn_{\alpha,\beta}(\mathbf{r}) - \gamma_c] |\psi_{\alpha,\beta}(\mathbf{r})|^2 d^2\mathbf{r}$ , with  $N^{-1} = \int |\psi_{\alpha}(\mathbf{r})|^2 d^2\mathbf{r}$  [71]. The complex eigenvalues  $E_{\pm}$  of the corresponding effective two-level system, Eq. (2), can then be determined for a given  $\Delta\mathcal{E} = \mathcal{E}_{\alpha} - \mathcal{E}_{\beta}$  and as a function of the mode coupling strength  $\mu$  with the nonlinear energies as input for  $E_{\alpha,\beta}$ . For the coupled two-level NSE, Eq. (3), with  $\mu = \Delta\Gamma$  close to the degeneracy  $\Delta\mathcal{E} = 0$ , the two modes coalesce into the superposition mode in which a vortex-antivortex pair forms [see Fig. 1(e)]. We note that in our simulations, the superposition mode is resilient to a random disorder potential (explicitly tested for random external potentials with a correlation length of  $1\ \mu\text{m}$  and average depth of about  $0.1\ \text{meV}$ ). By encircling the EP, supported by  $P_2$ , the two vortices swap their topological charge, which is a typical property of a topological Riemann surface [71]. Details of the encircling are given in Appendix A 2 in Fig. 6.

### III. SENSING ENHANCEMENT

We first focus on the influence of nonlinearities on the complex eigenvalues along the degeneracy of real-valued mode energies  $\Delta\mathcal{E} = 0$ . The eigenvalues  $E_{\pm}$  of the two-dimensional system are determined as a function of  $\mu$  by evaluating the eigenvalues according to the method introduced above. Exposed to a saturable gain, which in our case is expressed by  $R|\psi(\mathbf{r})|^2$ , the gain difference of the modes in a nonlinear system depends on their intensities. The coupling of the modes in our multistable system is also influenced by the strength of the polariton-polariton interaction. Thus, the necessary coupling strength  $\mu$  to reach the EP in such a nonlinear system is changed by the intensity of the modes or, in this case, the two-dimensional polariton density. Hence, we observe a shift of the EP along the  $\Delta\Gamma$  or  $\mu$  axis as a function of the nonlinear interaction strength (see Fig. 5). A similar effect was recently observed in Ref. [37] in a lasing system. For stationary solutions with  $|\psi_{\alpha,\beta}|^2 = \max[|\psi_{\alpha,\beta}(\mathbf{r})|^2]$  and  $n_{\alpha,\beta} = \max[n_{\alpha,\beta}(\mathbf{r})]$ , the eigenvalues of Eq. (2) with respect to the nonlinear terms of Eq. (1) read

$$E_{\pm,\text{NL}} \approx \frac{[E_{\alpha} + E_{\beta} + g_c |\psi_{\text{tot}}|^2 + g_r n_{\text{tot}} + i(\Gamma_{\alpha} + \Gamma_{\beta})]}{2} \pm \frac{\sqrt{|\mu|^2 + (\Delta E_L + \Delta E_{\text{NL}} + i\Delta\Gamma)^2}}{2}. \quad (4)$$

Here, the polariton- and reservoir-polariton interactions induce an energy blueshift on the Riemann surface proportional to the total polariton  $|\psi_{\text{tot}}|^2 = |\psi_{\alpha}|^2 + |\psi_{\beta}|^2$  and reservoir density  $n_{\text{tot}} = n_{\alpha} + n_{\beta}$ .  $\Delta E_{\text{NL}} = g_c \Delta|\psi|^2 + g_r \Delta n$  is characterized by the density difference  $\Delta|\psi|^2 = |\psi_{\alpha}|^2 - |\psi_{\beta}|^2$  and  $\Delta n = n_{\alpha} - n_{\beta}$ . We note that the expression in Eq. (4) represents a scalar approximation of the problem described in

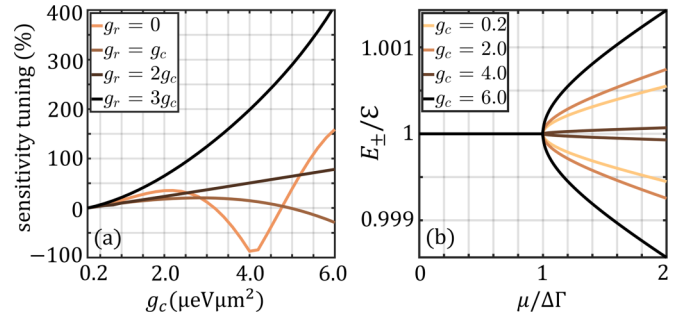


FIG. 2. Nonlinearity-induced enhancement of sensing at the EP. (a) Deviation of the eigenvalue splitting (real part) from the linear case at  $\mu/\Delta\Gamma = 2$ , close to the EP as a function of the polariton-polariton interaction  $g_c$  and for different polariton-reservoir interactions  $g_r$ . The values of the splitting deviation and the corresponding increased or decreased EP sensitivity are given as a percentage of the energy splitting in the linear case. (b) Eigenvalues  $E_{\pm}$  along the mode degeneracy line  $\Delta\mathcal{E} = 0$  for different interaction strengths  $g_c$  and  $g_r = 0$ , illustrating the change in the energy splitting. Eigenvalues are renormalized to the total mode energy  $\mathcal{E}$  at the EP.

Eq. (3). In this framework, the density of the modes is not subject to perturbation because the model describes the system in the vicinity of the EP, which limits the variation of the mode gain (see also details in Appendix A 1) and hence the density. From this discussion it follows that while the two modes coalesce at the EP with  $\Delta|\psi|^2 = 0$  and  $\Delta n = 0$ , tuning the system away from the EP also lifts the coalescence of the two modes, resulting in nonvanishing contributions of  $\Delta|\psi|^2$  and  $\Delta n$ . Depending on the exact shape of the two modes, this can lead to an increase ( $\Delta E_{\text{NL}} > 0$ ) or decrease ( $\Delta E_{\text{NL}} < 0$ ) of the eigenvalue splitting. The sensitivity change  $\kappa$  for a given ratio  $\mu/\Delta\Gamma$  can be derived as discussed in Appendix A 1.

After Eq. (3) is solved, the eigenvalues of Eq. (2) are calculated. Then their splitting  $\kappa$  is determined for  $\mu/\Delta\Gamma = 2$ , and the percentage deviation from the splitting at the reference value is calculated. The results are plotted in Fig. 2(a) as a function of  $g_c$  for different  $g_r$ . For  $g_r = 0$ , the sensitivity of the EP can increase by up to 150% and decrease to about 10%. For comparison, the resulting EPs are shown renormalized by their respective mode energies at  $\Delta\mathcal{E} = 0$  and their gain differences [see Fig. 2(b)]. For  $g_r \neq 0$ , the oscillation of the sensitivity decreases. For values of  $g_r \geq 2g_c$ , the sensitivity increases monotonically as the reservoir interaction dominates. It is worth pointing out that  $g_c$  depends on the detuning of the exciton and photon states and the choice of material [78] and can be controlled during sample preparation or in certain systems by applying a static electric field [64–66].

We note that the results shown here can also be validated with the dissipative Gross-Pitaevskii model in Eq. (1) once the EP is localized in the parameter space. There, the time evolution initialized with the third or fourth mode yields the superposition mode at the EP. In order not to duplicate results already shown in Fig. 1(e), the results of the GP model calculation are not shown explicitly. In essence, we find that the approximations introduced above for the derivation and evaluation of a simplified model description and the reduction to the third and fourth modes in the framework of the effective

Hamiltonian in Eq. (2) can also be applied to our nonlinear system in the vicinity of said EP, validating the model in Eq. (3). The added value of our model, which focuses on the relevant parameter domain and relevant modes, lies in its simplicity and low dimension. This renders the localization of the EP in the parameter space of the nonlinear system easier and the analysis more systematic and less specific to the particular physical system investigated here.

#### IV. RIEMANN SURFACE ROTATION

We extend our investigation from the bifurcation of the eigenvalues at the EP along the trace of degeneracy to the entire Riemann surface in the nonlinear regime. Here, we determine the eigenvalues by using Eq. (4) depending on  $\Delta E_L$  and  $\Delta\Gamma$ . Spatially varying quantities are replaced by scalar approximations. Thus, the flat top pump  $P$  is approximated by its peak intensity  $I_1$ , and the mode densities are approximated by their average values  $|\bar{\psi}|^2 \approx 3 \mu\text{m}^{-2}$  inside the external potential.  $E_\alpha$  is fixed to the eigenenergy of the dipole mode, as shown in Fig. 1(c), while  $E_\beta$  is varied close to this value. The resulting energy difference is linked to the ratio of the length and width of the rectangular potential [70]. The mode coupling is extracted from the calculations performed in the previous section. To construct the Riemann surface, the gain and loss difference is varied independently. To this end, we assume that the total density  $|\psi_{\text{tot}}|^2$  is resilient to small variations of  $\Delta\Gamma$ . The remaining parameters are taken from the GP model calculations. The nonlinear correction to the energy difference  $\Delta E_{\text{NL}} = g_c \Delta|\psi|^2$  is determined by deriving an expression for the polariton density contrast resulting from a gain and loss difference  $\Delta\Gamma$ , which reads (details are given in Appendix A 3)

$$\Delta|\psi|^2 = \frac{2\Delta\Gamma}{\left[\frac{\hbar PR}{\gamma_c} - \hbar\gamma_c\right] + \sum_{m=2}^{\infty} \frac{\hbar PR^m}{\gamma_c^m} (-|\psi_{\text{tot}}|^2)^{m-1}}. \quad (5)$$

The terms within the sum in the denominator follow from the Taylor series of the average gain and loss difference  $\bar{\Gamma} = \frac{\hbar}{2} \left[ \frac{RP}{\gamma_c + R|\psi|^2} - \gamma_c \right] |\psi|^2$ , including the saturable gain. For the following study, we consider terms up to  $m = 6$ . Note that the density difference  $\Delta|\psi|^2$ , which mainly depends on  $\Delta\Gamma$ , has to be in a reasonable range for convergence. The influence of the Kerr-type nonlinearity  $|\psi|^2\psi$  and the saturable gain  $R|\psi|^2$  on the Riemann surface is illustrated in Fig. 3. Remarkably, the Kerr-type nonlinearity causes the trace of  $\Delta\mathcal{E} = 0$  not to be parallel to the  $\Delta\Gamma$  axis, which leads to rotation of the Riemann surface. In the presence of the saturable gain the rotation angle becomes density dependent and can thus be increased even further [see Figs. 3(a)–3(c)]; the nonlinearity-induced blueshift leads to a tilting of the  $\Delta\mathcal{E} = 0$  trace and movement of the EP. In the particular case of the polariton condensate, the polariton-reservoir interaction  $g_r$  can induce an additional blueshift and thus a rotation of the Riemann surface, as shown in Figs. 3(d)–3(f). The relation between the total reservoir density and the reservoir density difference derived from Eq. (5) is discussed in detail in Appendix A3. It shows that the Riemann surface can even be rotated into the opposite direction by virtue of the polariton-reservoir interaction. In polariton condensates the pump intensity can control

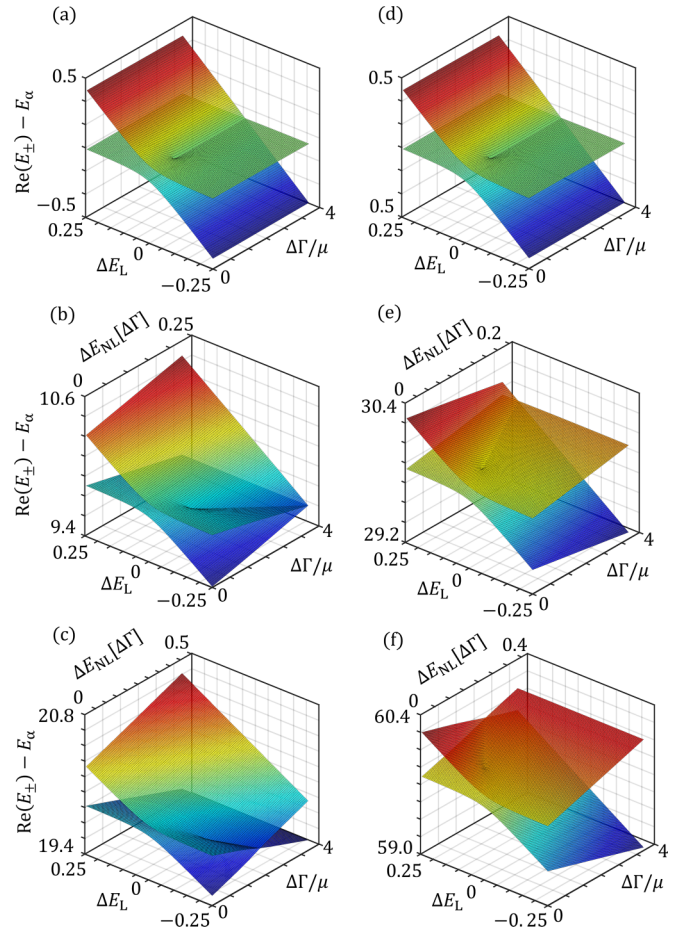


FIG. 3. Nonlinearity-induced rotation of Riemann surfaces. Riemann surfaces (real parts) resulting from the eigenvalue calculations, Eq. (4), for (a)–(c)  $g_r = 0$  and (d)–(f)  $g_r = 2g_c$  for different polariton-polariton interactions: (a) and (d)  $g_c = 0 \mu\text{eV} \mu\text{m}^2$ , (b) and (e)  $g_c = 3 \mu\text{eV} \mu\text{m}^2$  and (c) and (f)  $g_c = 6 \mu\text{eV} \mu\text{m}^2$ . The eigenvalues are depicted against the energy difference  $\Delta E_L$  and relative gain and loss difference  $\Delta\Gamma/\mu$ . For  $g_c \neq 0$  the nonlinear correction  $\Delta E_{\text{NL}}$  to the energy difference is plotted with  $\Delta\Gamma$ . Energies are given in  $\mu\text{eV}$ .

both nonlinear effects by tuning the density of the polariton condensate, which can provide an efficient method to actively tweak the spectral topology and the corresponding EP since in this case no other system parameters need to be varied.

From the rotation of the Riemann surface, it is worth asking whether more complicated higher-order EPs and multiple layer Riemann surfaces can also be manipulated. Here, we consider a parametrized and general three-level non-Hermitian Hamiltonian (with no direct relation to the specific modes in Fig. 1), as motivated by a linear system in Ref. [79], which reads

$$H_{\text{EP3}} = \begin{pmatrix} \mathcal{E}_\alpha + i\Gamma_\alpha & \mu_{\alpha\beta}/2 & 0 \\ \mu_{\alpha\beta}/2 & \mathcal{E}_\beta + i\Gamma_\beta & \mu_{\beta\gamma}/2 \\ 0 & \mu_{\beta\gamma}/2 & \mathcal{E}_\gamma + i\Gamma_\gamma \end{pmatrix}. \quad (6)$$

$\mathcal{E} = E + g_c|\psi|^2$  denotes the mode energy with nonlinearity. The mode energies  $E_\alpha$  and  $E_\beta$  and their coupling  $\mu_{\alpha\beta}$  refer to the values used above, while  $E_\gamma$  is set to  $1.75 \text{ meV}$  and  $\mu_{\beta\gamma} = 0.75\mu_{\alpha\beta}$ , providing a clear picture of the resulting

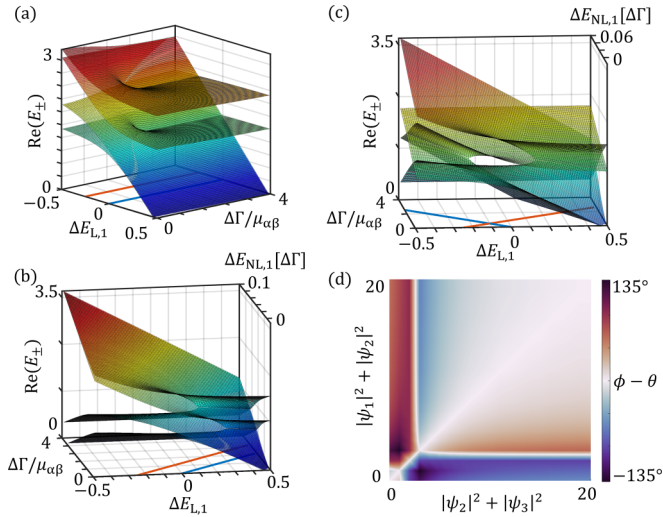


FIG. 4. Rotation of the Riemann surfaces with higher-order EPs. Riemann surfaces (real parts) containing two EPs (a) in the linear regime and (b) and (c) under the impact of the polariton-polariton interaction  $g_c = 6 \mu\text{eV} \mu\text{m}^2$  and the saturable gain. In (b) the total densities of the modes forming the EPs are identical, whereas in (c) the total densities inside each EP are distinct. The eigenvalues are depicted against the eigenenergy difference  $E_L$  and the gain and loss difference  $\Delta\Gamma$ . For  $g_c \neq 0$  the nonlinear correction to the energy difference is plotted with  $\Delta\Gamma$ . The lines at the bottom of the surface plot illustrate the orientation of the  $\Delta\mathcal{E} = 0$  trace to visualize the rotation of the Riemann surfaces. (d) Deflection angle of the two projected lines as a function of the total densities of the adjacent modes for a nonlinearity of  $g_c = 6 \mu\text{eV} \mu\text{m}^2$ . Energies are given in meV.

Riemann surfaces. In Figs. 4(a)–4(c), the Riemann surfaces are shown for different nonlinear contributions. Here, the traces  $\Delta\mathcal{E}_{1,2} = 0$  are projected onto the bottom of the surface plots to indicate the rotation of the Riemann surfaces. Remarkably, the Riemann surfaces can be rotated as a whole with the two projected lines being parallel [Figs. 4(a) and 4(b)]. Due to the saturable gain, however, the two Riemann surfaces can also be moved towards opposite directions with the two lines crossing each other [Fig. 4(c)], leading to complicated intersection behavior of the Riemann surfaces. Figure 4(d) shows the displacement angle difference of the two projected lines in Figs. 4(a)–4(c) as a function of the total densities of the two adjacent modes. It can be seen that if the saturable gain of the system is negligible or is identical for both EPs, the two lines are not deflected against each other, whereas they are deflected otherwise. It can also be inferred that if the energy blueshift is significant for one or two modes, it may be possible to observe coalescence of the two EPs, consequently leading to a phase transition in the spectral topology.

## V. CONCLUSION

We have investigated the influence of nonlinearity on non-Hermitian spectral topology in microcavity polariton condensates. The nonlinearities lead to a significant change in the eigenvalue splitting near the EP as a function of density difference, leading to a clear nonlinearity-induced sensing

capability enhancement. The Kerr-type nonlinearity of the condensate (from polariton-polariton interactions) and the saturable gain (from polariton-reservoir interactions) lead to a rotation of the Riemann surfaces and shift the EP in parameter space. This can give rise to a complex intersection pattern of Riemann surfaces for higher-order EPs. In nonlinear mode control this offers interesting insights for encircling higher-order EPs and for phase transitions at EPs. These results are generic enough to be applied to other non-Hermitian systems with similar nonlinearities such as in nonlinear optics and atomic systems.

## ACKNOWLEDGMENTS

This work was supported by the Deutsche Forschungsgemeinschaft (DFG) through Grants No. 467358803 and No. 519608013 and the transregional collaborative research center TRR142/3-2022 (231447078, Project No. A04) and by the Paderborn Center for Parallel Computing, PC<sup>2</sup>. We thank T. Gao for fruitful discussions.

## APPENDIX

This Appendix is structured as follows. In Appendix A1, the EP shift along the  $\Delta\Gamma$  or  $\mu$  axis is presented, and the expression for the sensitivity change  $\kappa$  in the vicinity of the EP is derived and introduced. In Appendix A2, the encircling of the EP and the resulting vortex-antivortex switching process are discussed. In Appendix A3, the derivation of the relevant equations for Riemann surface rotation is given.

### 1. EP shift and sensitivity tuning

With saturable gain, the gain difference of the modes in a nonlinear system depends on their intensity. Since the coupling of the modes in the multistable system is also affected by the strength of the polariton-polariton interaction  $g_c$ , the necessary coupling strength  $\mu$  to achieve an EP at  $\mu = \Delta\Gamma$  in such a nonlinear system depends on the intensity of the modes or, in this case, on the two-dimensional polariton density. Hence, we observe a shift of the EP along the  $\Delta\Gamma$  or  $\mu$  axis, as shown in Fig. 1(a), as a function of the nonlinear interaction strength  $g_c$ , as shown in Fig. 5. The EP position in parameter space is shown on the  $x$  axis, and the polariton-polariton interaction-strength parameter  $g_c$  is plotted on the  $y$  axis. It can be seen that the gain and loss difference of the two modes not only increases or decreases but can also switch sign for increasing (Kerr-type) nonlinearity.

In the vicinity of an EP in a system subject to a Kerr-type nonlinearity the sensitivity change  $\kappa$  for a given ratio  $\mu/\Delta\Gamma$  can be derived from Eq. (4) for  $\Delta E_L \approx 0$  and reads

$$\begin{aligned} \kappa &= \pm \frac{\sqrt{|\frac{\mu}{\Delta\Gamma}|^2 + (g_c \Delta|\psi|^2 + g_r \Delta n + i\Delta\Gamma)^2}}{2\mathcal{E}} \\ &\mp \frac{\sqrt{|\frac{\mu}{\Delta\Gamma'}|^2 - \Delta\Gamma'^2}}{2\mathcal{E}'}. \end{aligned} \quad (\text{A1})$$

Here, the  $\pm$  and  $\mp$  signs describe the eigenvalue splitting in both directions. The first term describes the eigenvalue splitting under the influence of the nonlinear interactions  $g_c$  and

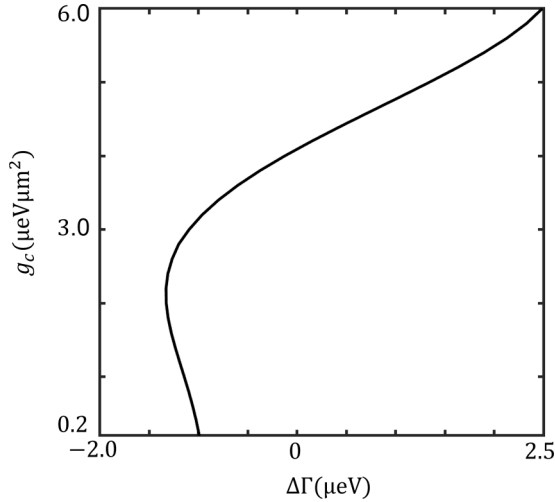


FIG. 5. Nonlinearity-induced shift of the required gain difference  $\Delta\Gamma$  to access the EP. Inverted plot to illustrate the EP-position ( $x$ -axis) shifting in parameter space under variation of the nonlinearity parameter  $g_c$ .

$g_r$ , while the second term describes the eigenvalue splitting in the linear case. The resulting EPs are superimposed by renormalizing the two scenarios with the respective mode energies  $\mathcal{E}$  and  $\mathcal{E}'$  at  $\Delta\mathcal{E} = 0$  and their gain differences  $\Delta\Gamma$  and  $\Delta\Gamma'$ . Since multistability of modes is required in the system under investigation, the eigenvalue bifurcation for a weak nonlinearity of  $g_c = 0.2 \mu\text{eV} \mu\text{m}^2$  is chosen as a reference value for the sensitivity tuning in Fig. 2(a).

## 2. EP encircling

The encircling of an EP and the resulting state transitions, including the accumulation of geometric Berry phases, were originally discussed in Ref. [80]. Here, for completeness, we show that in the system studied in the present work, the encircling process can lead to a change in the topological charge of the vortex-antivortex pair upon reentry into the EP. To this end, the width of the rectangular potential is slightly reduced to  $8.7 \mu\text{m}$  to lift the degeneracy of the two modes. This shifts the tripole mode [Fig. 1(d)] above the dipole mode [Fig. 1(c)] of the system. In addition to the excitation pump  $P_1(x, y)$ , a second elliptical control pump  $P_2(\mathbf{r})$  is introduced. The total pump profile is then given as

$$P(x, y) = I_1 \exp\left(-\frac{x^2 + y^2}{\sigma^2}\right)^6 + I_2 \exp\left(-\left|\frac{x^2}{\sigma_x^2} + \frac{y^2}{\sigma_y^2}\right|\right)^2. \quad (\text{A2})$$

Here,  $I_1 = [14; 16] \text{ps}^{-1} \mu\text{m}^{-2}$  and  $\sigma = 12 \mu\text{m}$  describe the intensity and width of the excitation pump. The shape of the elliptic pump is defined by its width  $\sigma_x = 5 \mu\text{m}$  in the  $x$  direction and  $\sigma_y = 2 \mu\text{m}$  in the  $y$  direction.  $I_2 = [0; 2] \text{ps}^{-1} \mu\text{m}^{-2}$  describes the intensity of the elliptic pump. Since the saturable gain affects the gain difference of the two modes, the excitation pump is used in the following to control these differences. In addition, the elliptic pump induces a spatially modulated blueshift which, due to its shape, mainly affects the dipole mode of the system. Thus, both the energy and gain difference of the modes can be controlled, which allows for an encircling of the EP that is induced all optically.

We note that in this case the encircling trajectories are not parallel to the  $\Delta E$  and  $\Delta\Gamma$  axes since both pumps cause an individual blueshift and gain shift to the two modes. Figure 6 shows the first and second encircling processes. It is emphasized that due to the nonlinearity of the system, the states exemplified at the corners of the encircling process are stationary before converging to the EP mode. During the first encircling, the dipole mode gathers a  $-\pi$  Berry phase, while the tripole mode and hence the EP mode remain unchanged. Only after a second encircling does the tripole mode also collect a geometric Berry phase, leading to the switching of the topological charge of the vortex-antivortex pair.

## 3. Mathematical description of the Riemann surface rotation

To describe the rotation of the Riemann surface in the nonlinear regime as shown in Fig. 3, the expression for  $\Delta|\psi|^2$  depending on  $\Delta\Gamma$  can be derived by performing the Taylor expansion on the average mode gain and loss ratio  $\bar{\Gamma} = \frac{\hbar}{2} \left[ \frac{RP}{\gamma_r + R|\bar{\psi}|^2} - \gamma_c \right] |\bar{\psi}|^2$  at  $|\bar{\psi}|^2 = 0$  given the approximation of constant average polariton density  $|\bar{\psi}|^2$  and pump intensity  $P = I_1$ . The series expansion converges for  $|\bar{\psi}|^2 < \gamma_r/R$ . We note that this does not limit the strength of nonlinearity that can be studied within this approximation, as  $g_c$  can be tuned freely to model strong nonlinear effects. The Taylor expansion of the gain and loss ratio reads

$$\bar{\Gamma} = \frac{\hbar}{2} \left( \left[ \frac{RP}{\gamma_r} - \gamma_c \right] |\bar{\psi}|^2 - \frac{PR^2}{\gamma_r^2} |\bar{\psi}|^4 + \frac{PR^3}{\gamma_r^3} |\bar{\psi}|^6 \mp \dots \right). \quad (\text{A3})$$

From this the mode density difference of the two modes,  $\alpha$  and  $\beta$ , as a function of their gain and loss difference can be derived as

$$\begin{aligned} \Delta\Gamma &= \frac{\hbar}{2} \left( \left[ \frac{RP}{\gamma_r} - \gamma_c \right] (|\bar{\psi}_\alpha|^2 - |\bar{\psi}_\beta|^2) - \frac{PR^2}{\gamma_r^2} (|\bar{\psi}_\alpha|^4 - |\bar{\psi}_\beta|^4) + \frac{PR^3}{\gamma_r^3} (|\bar{\psi}_\alpha|^6 - |\bar{\psi}_\beta|^6) \mp \dots \right) \\ \Leftrightarrow \Delta\Gamma &= \frac{\hbar}{2} \left( \left[ \frac{RP}{\gamma_r} - \gamma_c \right] \Delta|\psi|^2 - \frac{PR^2}{\gamma_r^2} (|\bar{\psi}_\alpha|^2 + |\bar{\psi}_\beta|^2) \Delta|\psi|^2 + \frac{PR^3}{\gamma_r^3} (|\bar{\psi}_\alpha|^4 + |\bar{\psi}_\alpha|^2 |\bar{\psi}_\beta|^2 + |\bar{\psi}_\beta|^4) \Delta|\psi|^2 \mp \dots \right) \\ \Leftrightarrow \Delta|\psi|^2 [\Delta\Gamma] &= \frac{2\Delta\Gamma}{\left[ \frac{\hbar RP}{\gamma_r} - \hbar\gamma_c \right] - \frac{\hbar PR^2}{\gamma_r^2} (|\bar{\psi}_\alpha|^2 + |\bar{\psi}_\beta|^2) + \frac{\hbar PR^3}{\gamma_r^3} (|\bar{\psi}_\alpha|^4 + |\bar{\psi}_\beta|^2 |\bar{\psi}_\beta|^2 + |\bar{\psi}_\beta|^4) \mp \dots} \end{aligned}$$

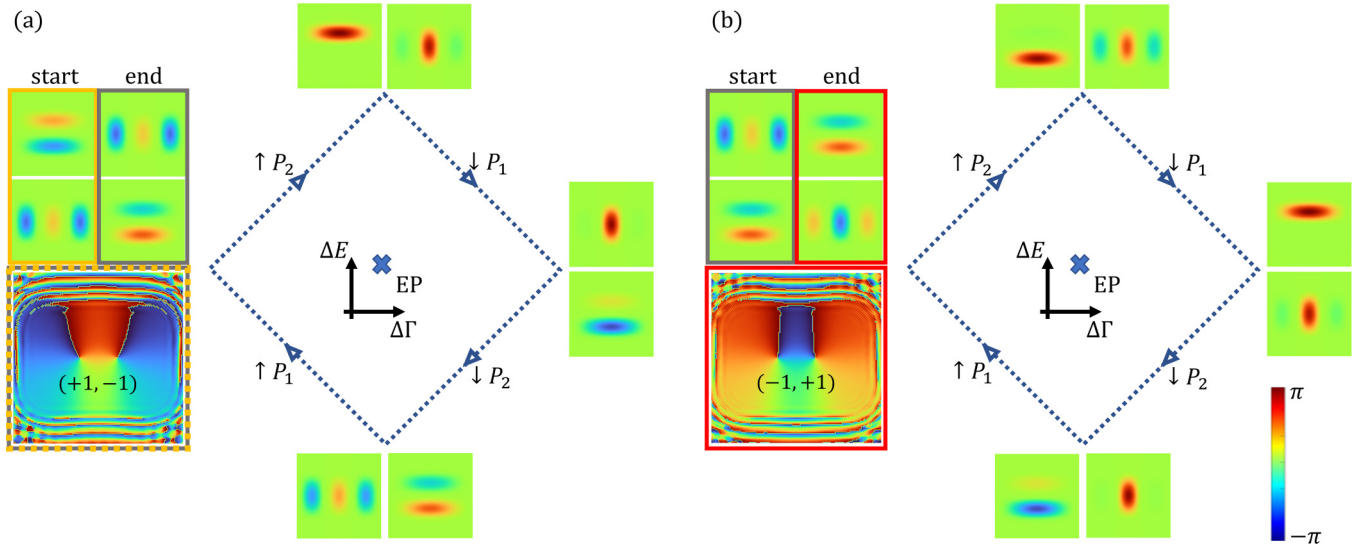


FIG. 6. All-optical vortex-antivortex switching under EP encircling. Illustration of the (a) first and (b) second EP encirclings. The contours of the stationary states are displayed at the corners of the sketched trajectory. The initial and final states are highlighted, and the phase information of the vortex-antivortex pair at the EP is displayed at the bottom. After the first encircling the topological charge of the vortex pair remains unchanged (highlighted by gray and yellow boxes). After the second encircling the topological charge of the vortex pair is switched (highlighted by a red box).

$$\begin{aligned} \Rightarrow \Delta|\psi|^2[\Delta\Gamma] &\approx \frac{2\Delta\Gamma}{\left[\frac{\hbar RP}{\gamma_r} - \hbar\gamma_c\right] - \frac{\hbar PR^2}{\gamma_r^2}(|\bar{\psi}_\alpha|^2 + |\bar{\psi}_\beta|^2) + \frac{\hbar PR^3}{\gamma_r^3}(|\bar{\psi}_\alpha|^2 + |\bar{\psi}_\beta|^2)^2 \mp \dots} \\ \Rightarrow \Delta|\psi|^2[\Delta\Gamma] &\approx \frac{2\Delta\Gamma}{\left[\frac{\hbar PR}{\gamma_r} - \hbar\gamma_c\right] + \sum_{m=2}^{\infty} (-1)^{m-1} \frac{\hbar PR^m}{\gamma_r^m} (|\psi_{\text{tot}}|^2)^{m-1}}. \end{aligned}$$

In the second step, the terms of the form  $(|\bar{\psi}_\alpha|^2)^m - (|\bar{\psi}_\beta|^2)^m$  are factorized with respect to the density difference  $\Delta|\psi|^2$ , according to

$$x^m - y^m = (x - y) \sum_{l=0}^{m-1} x^l y^{m-1-l}. \quad (\text{A4})$$

In the last step, the factors of the  $m$ th-order terms are approximated by the total density  $\psi_{\text{tot}} = |\psi_\alpha|^2 + |\psi_\beta|^2$  to the  $(m - 1)$ th power. By this approximation, the denominator is always larger than its exact value for the parameter range bounded by the Taylor expansion. Accordingly, this approximation describes a lower bound for the mode density difference under the independent variation of  $\Delta\Gamma$ . We emphasize that this approximation is exact for the first two terms in the denominator and the strengths of the higher-order terms decrease by one order of magnitude for each order  $m$ . In this sense this approximation does not significantly affect our results. We note that the denominator vanishes when the saturable gain compensates the linear gain. For larger densities the direction of the rotation is inverted. Keeping in mind the approximations discussed above, we collect our results away from this divergence.

To determine the rotation and blueshift of the Riemann surface [see Eq. (4)] induced by the excitation reservoir  $n$  in a polariton system, we derive the expression for  $\Delta n[\Delta|\psi|^2]$  and  $n_{\text{tot}}[|\psi_{\text{tot}}|^2]$  from the Taylor expansion of  $\bar{\Gamma}$  in Eq. (A3) and the relation  $\bar{\Gamma} = \frac{\hbar}{2}[Rn - \gamma_c]|\bar{\psi}|^2$ . The blueshift  $g_r n_{\text{tot}}$  of the Riemann surface is then derived as

$$g_r n_{\text{tot}} = g_r \left( \left[ \frac{2P}{\gamma_r} - \frac{2\gamma_c}{R} \right] + \sum_{m=1}^{\infty} (-1)^m \frac{PR^m}{\gamma_r^{m+1}} (|\psi_{\text{tot}}|^2)^m \right). \quad (\text{A5})$$

The rotation induced by the excitation reservoir is given by

$$\Delta n = \sum_{m=1}^{\infty} (-1)^m \frac{PR^m}{\gamma_r^{m+1}} (|\psi_{\text{tot}}|^2)^{m-1} \Delta|\psi|^2. \quad (\text{A6})$$

From the given expression and the results shown in Figs. 3(e) and 3(f) it can be seen that the rotation induced by the reservoir not only can increase the rotation angle of the Riemann surface but can also switch the rotation direction, depending on the density and reservoir differences.

[1] M. V. Berry, Physics of non-Hermitian degeneracies, *Czech. J. Phys.* **54**, 1039 (2004).

[2] W. Heiss, Exceptional points of non-Hermitian operators, *J. Phys. A* **37**, 2455 (2004).

- [3] C. M. Bender, Making sense of non-Hermitian Hamiltonians, *Rep. Prog. Phys.* **70**, 947 (2007).
- [4] W. D. Heiss, The physics of exceptional points, *J. Phys. A* **45**, 444016 (2012).
- [5] T. Kato, *Perturbation Theory for Linear Operators*, Classics in Mathematic Vol. 132 (Springer, Berlin, Heidelberg, 2013).
- [6] J. Wiersig, Nonorthogonality constraints in open quantum and wave systems, *Phys. Rev. Res.* **1**, 033182 (2019).
- [7] M.-A. Miri and A. Alù, Exceptional points in optics and photonics, *Science* **363**, eaar7709 (2019).
- [8] K. Ding, C. Fang, and G. Ma, Non-Hermitian topology and exceptional-point geometries, *Nat. Rev. Phys.* **4**, 745 (2022).
- [9] C. Dembowski, H.-D. Gräf, H. L. Harney, A. Heine, W. D. Heiss, H. Rehfeld, and A. Richter, Experimental observation of the topological structure of exceptional points, *Phys. Rev. Lett.* **86**, 787 (2001).
- [10] C. Dembowski, B. Dietz, H.-D. Gräf, H. L. Harney, A. Heine, W. D. Heiss, and A. Richter, Observation of a chiral state in a microwave cavity, *Phys. Rev. Lett.* **90**, 034101 (2003).
- [11] H. Cao and J. Wiersig, Dielectric microcavities: Model systems for wave chaos and non-Hermitian physics, *Rev. Mod. Phys.* **87**, 61 (2015).
- [12] Y. Choi, S. Kang, S. Lim, W. Kim, J.-R. Kim, J.-H. Lee, and K. An, Quasieigenstate coalescence in an atom-cavity quantum composite, *Phys. Rev. Lett.* **104**, 153601 (2010).
- [13] A. Kodigala, T. Lepetit, and B. Kanté, Exceptional points in three-dimensional plasmonic nanostructures, *Phys. Rev. B* **94**, 201103(R) (2016).
- [14] J.-H. Park, A. Ndao, and B. Kanté, Observation of exceptional points in passive plasmonic nanostructure, in *Frontiers in Optics* (Optical Society of America, Washington, DC, 2019), pp. JTu4A–79.
- [15] A. Guo, G. J. Salamo, D. Duchesne, R. Morandotti, M. Volatier-Ravat, V. Aimez, G. A. Siviloglou, and D. N. Christodoulides, Observation of  $\mathcal{PT}$ -symmetry breaking in complex optical potentials, *Phys. Rev. Lett.* **103**, 093902 (2009).
- [16] S.-B. Lee, J. Yang, S. Moon, S.-Y. Lee, J.-B. Shim, S. W. Kim, J.-H. Lee, and K. An, Observation of an exceptional point in a chaotic optical microcavity, *Phys. Rev. Lett.* **103**, 134101 (2009).
- [17] L. Chang, X. Jiang, S. Hua, C. Yang, J. Wen, L. Jiang, G. Li, G. Wang, and M. Xiao, Parity-time symmetry and variable optical isolation in active-passive-coupled microresonators, *Nat. Photonics* **8**, 524 (2014).
- [18] B. Peng, Ş. K. Özdemir, F. Lei, F. Monifi, M. Gianfreda, G. L. Long, S. Fan, F. Nori, C. M. Bender, and L. Yang, Parity-time-symmetric whispering-gallery microcavities, *Nat. Phys.* **10**, 394 (2014).
- [19] M. Fruchart, R. Hanai, P. B. Littlewood, and V. Vitelli, Non-reciprocal phase transitions, *Nature (London)* **592**, 363 (2021).
- [20] H. Zhang, F. Saif, Y. Jiao, and H. Jing, Loss-induced transparency in optomechanics, *Opt. Express* **26**, 25199 (2018).
- [21] H. Lü, C. Wang, L. Yang, and H. Jing, Optomechanically induced transparency at exceptional points, *Phys. Rev. Appl.* **10**, 014006 (2018).
- [22] Z. Lin, H. Ramezani, T. Eichelkraut, T. Kottos, H. Cao, and D. N. Christodoulides, Unidirectional invisibility induced by  $\mathcal{PT}$ -symmetric periodic structures, *Phys. Rev. Lett.* **106**, 213901 (2011).
- [23] W. Chen, Ş. Kaya Özdemir, G. Zhao, J. Wiersig, and L. Yang, Exceptional points enhance sensing in an optical microcavity, *Nature (London)* **548**, 192 (2017).
- [24] H. Hodaiei, A. U. Hassan, S. Wittek, H. Garcia-Gracia, R. El-Ganainy, D. N. Christodoulides, and M. Khajavikhan, Enhanced sensitivity at higher-order exceptional points, *Nature (London)* **548**, 187 (2017).
- [25] J. Wiersig, Review of exceptional point-based sensors, *Photonics Res.* **8**, 1457 (2020).
- [26] I. Mandal and E. J. Bergholtz, Symmetry and higher-order exceptional points, *Phys. Rev. Lett.* **127**, 186601 (2021).
- [27] J. Wiersig, Enhancing the sensitivity of frequency and energy splitting detection by using exceptional points: Application to microcavity sensors for single-particle detection, *Phys. Rev. Lett.* **112**, 203901 (2014).
- [28] J. Wiersig, Sensors operating at exceptional points: General theory, *Phys. Rev. A* **93**, 033809 (2016).
- [29] J. Wiersig, Prospects and fundamental limits in exceptional point-based sensing, *Nat. Commun.* **11**, 2454 (2020).
- [30] Z. Li, C. Li, Z. Xiong, G. Xu, Y. R. Wang, X. Tian, X. Yang, Z. Liu, Q. Zeng, R. Lin, Y. Li, J. K. W. Lee, J. S. Ho, and C.-W. Qiu, Stochastic exceptional points for noise-assisted sensing, *Phys. Rev. Lett.* **130**, 227201 (2023).
- [31] A. U. Hassan, H. Hodaiei, M.-A. Miri, M. Khajavikhan, and D. N. Christodoulides, Nonlinear reversal of the  $\mathcal{PT}$ -symmetric phase transition in a system of coupled semiconductor microring resonators, *Phys. Rev. A* **92**, 063807 (2015).
- [32] L. Ge and R. El-Ganainy, Nonlinear modal interactions in parity-time ( $\mathcal{PT}$ ) symmetric lasers, *Sci. Rep.* **6**, 24889 (2016).
- [33] Y. Kominis, V. Kovanis, and T. Bountis, Controllable asymmetric phase-locked states of the fundamental active photonic dimer, *Phys. Rev. A* **96**, 043836 (2017).
- [34] M. H. Teimourpour, M. Khajavikhan, D. N. Christodoulides, and R. El-Ganainy, Robustness and mode selectivity in parity-time ( $\mathcal{PT}$ ) symmetric lasers, *Sci. Rep.* **7**, 10756 (2017).
- [35] A. Nikzamir and F. Capolino, Highly sensitive coupled oscillator based on an exceptional point of degeneracy and nonlinearity, *Phys. Rev. Appl.* **18**, 054059 (2022).
- [36] S. Ramezanpour and A. Bogdanov, Tuning exceptional points with Kerr nonlinearity, *Phys. Rev. A* **103**, 043510 (2021).
- [37] K. Ji, Q. Zhong, L. Ge, G. Beaudoin, I. Sagnes, F. Raineri, R. El-Ganainy, and A. M. Yacomotti, Tracking exceptional points above laser threshold, [arXiv:2212.06488](https://arxiv.org/abs/2212.06488).
- [38] H. Wang, S. Assaworrorarit, and S. Fan, Dynamics for encircling an exceptional point in a nonlinear non-Hermitian system, *Opt. Lett.* **44**, 638 (2019).
- [39] P. Senellart and J. Bloch, Nonlinear emission of microcavity polaritons in the low density regime, *Phys. Rev. Lett.* **82**, 1233 (1999).
- [40] L. S. Dang, D. Heger, R. André, F. Bœuf, and R. Romestain, Stimulation of polariton photoluminescence in semiconductor microcavity, *Phys. Rev. Lett.* **81**, 3920 (1998).
- [41] P. G. Savvidis, J. J. Baumberg, R. M. Stevenson, M. S. Skolnick, D. M. Whittaker, and J. S. Roberts, Angle-resonant stimulated polariton amplifier, *Phys. Rev. Lett.* **84**, 1547 (2000).
- [42] C. Ciuti, P. Schwendimann, B. Deveaud, and A. Quattropani, Theory of the angle-resonant polariton amplifier, *Phys. Rev. B* **62**, R4825 (2000).



- [43] R. M. Stevenson, V. N. Astratov, M. S. Skolnick, D. M. Whittaker, M. Emam-Ismail, A. I. Tartakovskii, P. G. Savvidis, J. J. Baumberg, and J. S. Roberts, Continuous wave observation of massive polariton redistribution by stimulated scattering in semiconductor microcavities, *Phys. Rev. Lett.* **85**, 3680 (2000).
- [44] H. Deng, G. Weihs, C. Santori, J. Bloch, and Y. Yamamoto, Condensation of semiconductor microcavity exciton polaritons, *Science* **298**, 199 (2002).
- [45] J. Kasprzak, M. Richard, S. Kundermann, A. Baas, P. Jeambrun, J. M. J. Keeling, F. M. Marchetti, M. H. Szymańska, R. André, J. L. Staehli, V. Savona, P. B. Littlewood, B. Deveaud, and L. S. Dang, Bose–Einstein condensation of exciton polaritons, *Nature (London)* **443**, 409 (2006).
- [46] H. Deng, H. Haug, and Y. Yamamoto, Exciton-polariton Bose-Einstein condensation, *Rev. Mod. Phys.* **82**, 1489 (2010).
- [47] E. Wertz, L. Ferrier, D. D. Solnyshkov, R. Johne, D. Sanvitto, A. Lemaître, I. Sagnes, R. Grousson, A. V. Kavokin, P. Senellart, G. Malpuech, and J. Bloch, Spontaneous formation and optical manipulation of extended polariton condensates, *Nat. Phys.* **6**, 860 (2010).
- [48] D. Sanvitto, S. Pigeon, A. Amo, D. Ballarini, M. De Giorgi, I. Carusotto, R. Hivet, F. Pisanello, V. Sala, P. Guimaraes, R. Houdré, E. Giacobino, C. Ciuti, A. Bramati, and G. Gigli, All-optical control of the quantum flow of a polariton condensate, *Nat. Photonics* **5**, 610 (2011).
- [49] E. Wertz, A. Amo, D. D. Solnyshkov, L. Ferrier, T. C. H. Liew, D. Sanvitto, P. Senellart, I. Sagnes, A. Lemaître, A. V. Kavokin, G. Malpuech, and J. Bloch, Propagation and amplification dynamics of 1D polariton condensates, *Phys. Rev. Lett.* **109**, 216404 (2012).
- [50] P. Cristofolini, A. Dreismann, G. Christmann, G. Franchetti, N. G. Berloff, P. Tsotsis, Z. Hatzopoulos, P. G. Savvidis, and J. J. Baumberg, Optical superfluid phase transitions and trapping of polariton condensates, *Phys. Rev. Lett.* **110**, 186403 (2013).
- [51] A. Askitopoulos, H. Ohadi, A. V. Kavokin, Z. Hatzopoulos, P. G. Savvidis, and P. G. Lagoudakis, Polariton condensation in an optically induced two-dimensional potential, *Phys. Rev. B* **88**, 041308(R) (2013).
- [52] A. Amo, D. Sanvitto, F. Laussy, D. Ballarini, E. d. Valle, M. Martin, A. Lemaître, J. Bloch, D. Krizhanovskii, M. Skolnick, C. Tejedor, and L. Viña, Collective fluid dynamics of a polariton condensate in a semiconductor microcavity, *Nature (London)* **457**, 291 (2009).
- [53] G. Tosi, G. Christmann, N. Berloff, P. Tsotsis, T. Gao, Z. Hatzopoulos, P. Savvidis, and J. Baumberg, Sculpting oscillators with light within a nonlinear quantum fluid, *Nat. Phys.* **8**, 190 (2012).
- [54] R. Dall, M. D. Fraser, A. S. Desyatnikov, G. Li, S. Brodbeck, M. Kamp, C. Schneider, S. Höfling, and E. A. Ostrovskaya, Creation of orbital angular momentum states with chiral polaritonic lenses, *Phys. Rev. Lett.* **113**, 200404 (2014).
- [55] J. Schmutzler, P. Lewandowski, M. Aßmann, D. Niemietz, S. Schumacher, M. Kamp, C. Schneider, S. Höfling, and M. Bayer, All-optical flow control of a polariton condensate using nonresonant excitation, *Phys. Rev. B* **91**, 195308 (2015).
- [56] X. Ma, B. Berger, M. Aßmann, R. Driben, T. Meier, C. Schneider, S. Höfling, and S. Schumacher, Realization of all-optical vortex switching in exciton-polariton condensates, *Nat. Commun.* **11**, 897 (2020).
- [57] A. Baas, J.-P. Karr, M. Romanelli, A. Bramati, and E. Giacobino, Optical bistability in semiconductor microcavities in the nondegenerate parametric oscillation regime: Analogy with the optical parametric oscillator, *Phys. Rev. B* **70**, 161307(R) (2004).
- [58] N. A. Gippius, I. A. Shelykh, D. D. Solnyshkov, S. S. Gavrilov, Y. G. Rubo, A. V. Kavokin, S. G. Tikhodeev, and G. Malpuech, Polarization multistability of cavity polaritons, *Phys. Rev. Lett.* **98**, 236401 (2007).
- [59] T. Paraíso, M. Wouters, Y. Léger, F. Morier-Genoud, and B. Deveaud-Plédran, Multistability of a coherent spin ensemble in a semiconductor microcavity, *Nat. Mater.* **9**, 655 (2010).
- [60] X. Ma and S. Schumacher, Vortex multistability and Bessel vortices in polariton condensates, *Phys. Rev. Lett.* **121**, 227404 (2018).
- [61] D. Ballarini, M. De Giorgi, E. Cancellieri, R. Houdré, E. Giacobino, R. Cingolani, A. Bramati, G. Gigli, and D. Sanvitto, All-optical polariton transistor, *Nat. Commun.* **4**, 1778 (2013).
- [62] K. G. Lagoudakis, M. Wouters, M. Richard, A. Baas, I. Carusotto, R. André, L. S. Dang, and B. Deveaud-Plédran, Quantized vortices in an exciton-polariton condensate, *Nat. Phys.* **4**, 706 (2008).
- [63] J. Wingenbach, M. Pukrop, S. Schumacher, and X. Ma, Dynamics of phase defects trapped in optically imprinted orbits in dissipative binary polariton condensates, *Phys. Rev. B* **105**, 245302 (2022).
- [64] S. I. Tsintzos, A. Tzimis, G. Stavrinidis, A. Trifonov, Z. Hatzopoulos, J. J. Baumberg, H. Ohadi, and P. G. Savvidis, Electrical tuning of nonlinearities in exciton-polariton condensates, *Phys. Rev. Lett.* **121**, 037401 (2018).
- [65] J. De, X. Ma, F. Yin, J. Ren, J. Yao, S. Schumacher, Q. Liao, H. Fu, G. Malpuech, and D. Solnyshkov, Room-temperature electrical field-enhanced ultrafast switch in organic microcavity polariton condensates, *J. Am. Chem. Soc.* **145**, 1557 (2023).
- [66] X. Zhai, X. Ma, Y. Gao, C. Xing, M. Gao, H. Dai, X. Wang, A. Pan, S. Schumacher, and T. Gao, Electrically controlling vortices in a neutral exciton polariton condensate at room temperature, *Phys. Rev. Lett.* **131**, 136901 (2023).
- [67] X. Xu, R. Bao, and T. C. H. Liew, Non-Hermitian topological exciton-polariton corner modes, *Phys. Rev. B* **106**, L201302 (2022).
- [68] I. Septembre, S. Koniakhin, J. S. Meyer, D. D. Solnyshkov, and G. Malpuech, Parametric amplification of topological interface states in synthetic Andreev bands, *Phys. Rev. B* **103**, 214504 (2021).
- [69] C. Lee, K. Zhang, J. Miao, K. Sun, and H. Deng, Polariton-driven  $\mathcal{PT}$  reentry and anisotropic exceptional points in  $\mathcal{PT}$ -symmetric ternary system, *arXiv:2306.14065*.
- [70] T. Gao, E. Estrecho, K. Bliokh, T. Liew, M. Fraser, S. Brodbeck, M. Kamp, C. Schneider, S. Höfling, Y. Yamamoto, F. Nori, Y. S. Kivshar, A. Truscott, R. Dall, and E. Ostrovskaya, Observation of non-Hermitian degeneracies in a chaotic exciton-polariton billiard, *Nature (London)* **526**, 554 (2015).
- [71] T. Gao, G. Li, E. Estrecho, T. C. H. Liew, D. Comber-Todd, A. Nalitov, M. Steger, K. West, L. Pfeiffer, D. W. Snoke, A. V. Kavokin, A. G. Truscott, and E. A. Ostrovskaya, Chiral modes at exceptional points in exciton-polariton quantum fluids, *Phys. Rev. Lett.* **120**, 065301 (2018).
- [72] R. Hanai, A. Edelman, Y. Ohashi, and P. B. Littlewood, Non-Hermitian phase transition from a polariton Bose-Einstein

- condensate to a photon laser, *Phys. Rev. Lett.* **122**, 185301 (2019).
- [73] Z.-F. Yu, J.-K. Xue, L. Zhuang, J. Zhao, and W.-M. Liu, Non-Hermitian spectrum and multistability in exciton-polariton condensates, *Phys. Rev. B* **104**, 235408 (2021).
- [74] Y. Li, X. Ma, Z. Hatzopoulos, P. G. Savvidis, S. Schumacher, and T. Gao, Switching off a microcavity polariton condensate near the exceptional point, *ACS Photonics* **9**, 2079 (2022).
- [75] Q. Liao, C. Leblanc, J. Ren, F. Li, Y. Li, D. Solnyshkov, G. Malpuech, J. Yao, and H. Fu, Experimental measurement of the divergent quantum metric of an exceptional point, *Phys. Rev. Lett.* **127**, 107402 (2021).
- [76] M. Wouters and I. Carusotto, Excitations in a nonequilibrium Bose-Einstein condensate of exciton polaritons, *Phys. Rev. Lett.* **99**, 140402 (2007).
- [77] M. Carcamo, S. Schumacher, and R. Binder, Transfer function replacement of phenomenological single-mode equations in semiconductor microcavity modeling, *Appl. Opt.* **59**, G112 (2020).
- [78] E. Estrecho, T. Gao, N. Bobrovska, D. Comber-Todd, M. D. Fraser, M. Steger, K. West, L. N. Pfeiffer, J. Levinsen, M. M. Parish, T. C. H. Liew, M. Matuszewski, D. W. Snoke, A. G. Truscott, and E. A. Ostrovskaya, Direct measurement of polariton-polariton interaction strength in the Thomas-Fermi regime of exciton-polariton condensation, *Phys. Rev. B* **100**, 035306 (2019).
- [79] G. Demange and E.-M. Graefe, Signatures of three coalescing eigenfunctions, *J. Phys. A* **45**, 025303 (2012).
- [80] C. Dembowski, B. Dietz, H.-D. Gräf, H. L. Harney, A. Heine, W. D. Heiss, and A. Richter, Encircling an exceptional point, *Phys. Rev. E* **69**, 056216 (2004).